Hindawi Publishing Corporation
EURASIP Journal on Advances in Signal Processing
Volume 2008, Article ID 394219, 14 pages
doi:10.1155/2008/394219

Research Article

State Space Initiation for Blind Mobile Terminal Position Tracking

Vadim Algeier,[1] Bruno Demissie,[2] Wolfgang Koch,[2] and Reiner Thomä[1]

[1] *Electronic Measurement Research Lab, Institute of Information Technology, Ilmenau University of Technology, P.O. Box 100 565, 98684 Ilmenau, Germany*
[2] *Research Institute for Communication, Information Processing and Ergonomics (FKIE), Research Establishment for Applied Science (FGAN), Neuenahrer Straße 20, 53343 Wachtberg, Germany*

Correspondence should be addressed to Bruno Demissie, demissie@fgan.de

Received 23 April 2007; Accepted 19 September 2007

Recommended by Yvo Boers

Blind localization and tracking of mobile terminals in urban scenarios is an important requirement for offering new location-based services, handling emergency cases of nonsubscribed users, public safety, countering IEDs, and so forth. In this context, we propose a track-before-detect scheme taking explicitly advantage of multipath propagation in an urban terrain by using a priori information about the known locations of the main scattering objects such as buildings. This information is made available for localization and tracking by a real-time ray tracing technique based on a 2D geographic database. This allows the prediction of the directional and temporal structure of the received multipath components for an arbitrary transmitter position. We consider a single observing station where the direction and the relative time of arrival of the received multipath components can be estimated by an antenna array. By a likelihood function, which is algorithmically defined for a randomly distributed set of potential transmitter positions, these measurements are compared with those being expected by ray tracing. This likelihood function is the key component of a track-before-detect scheme providing initial state estimates for mobile transmitter tracking using a particle filtering technique.

1. INTRODUCTION

There is a rapid growth of wireless applications that require the knowledge of the mobile terminal's location [1]. For position estimation of mobile terminals in cellular networks there is a variety of methods that can be distinguished according to the respective underlying physical principles [2, 3]. All of them have pros and cons regarding accuracy, available coverage, cost, technical feasibility, and operational complexity in different environments and applications. Furthermore, they differ in the level of cooperation between the mobile terminal and the infrastructure or the other location reference stations. This makes them more or less suited for the variety of applications. Blind localization, for example, presumes no cooperation of the mobile terminal with the location reference station. This problem is typical of nonsubscribed user localization, for example, in emergency, security, and safety applications [4].

The first group of localization techniques is based on trilateration/triangulation utilizing received signal strength (RSS), time of arrival (ToA), time difference of arrival (TDoA), direction of arrival (DoA) of the signal, as well as diverse combinations of them [5, 6]. Some of these methods (ToA) require strict temporal synchronization between mobile station (MS) and the reference station. Others require synchronization or at least cooperation between the distributed reference stations (TDoA, DoA) which is no problem if they belong to the same network infrastructure. DoA estimation requires the usage of an antenna array at the base station (BS). All of those methods, however, presume line-of-sight (LoS) connection. Whereas in macrocell scenarios with elevated BSs frequently occuring LoS and near-LoS propagation give useful information on MS position [7], non-line-of-sight (NLoS) connection is predominant in urban scenarios if the BS is below roof top or just on street level. Although some methods of mitigating positioning error due to NLoS

were presented in the literature [2, 8], missing LoS still remains the major source of error of trilateration/triangulation based localization in urban scenarios.

Whereas missing LoS detrimentally affects the abovementioned techniques, there are methods available which can compensate this drawback by taking explicitly advantage of the multipath structure of wave propagation [7]. Fingerprint methods [9] belong to this group. They are based on some "comparison" of measured radio parameters, for example, channel impulse response (CIR) signature or DoA signature to precalculated or premeasured reference data. Correlation with premeasured data is most common for indoor scenarios [5] since high costs for creating the database exclude its application to outdoor scenarios. Moreover, precalculation of the reference data by application of ray tracing (RT) methods based upon an accurate database of the propagation environment constitutes extensive effort since all possible MS positions relative to the fixed reference position must be considered in advance. On the other hand, fingerprint methods are inherently well suited for single station localization (SSL) since they do not apply trilateration or triangulation. Instead, they compensate missing measured geometrical parameters by exploiting the a priori information about the geometric structure or the electromagnetic response of the environment. The method proposed in [4] uses blind estimates of DoA fingerprints at a single elevated BS (which simultaneously acts as observing station (OS)) that are compared to a dataset precalculated from a 3D geographic database by RT.

In this paper, the main goal is the blind localization/tracking of a mobile terminal at an OS that is not a part of the network infrastructure. Blind MS location estimation has different facets. Firstly, the spatial/temporal (DoA/ToA) structure of the channel (which is assumed to carry the information on the spatial location of the terminal relative to the observer position) has to be carried out without knowing details about the transmitted signal. Appropriate blind space-time-filtering techniques are required to estimate both the spatial and the temporal characteristics of the radio channel. Secondly, because of a lack of temporal synchronization between OS and MS, ToA estimation submits only excess (or relative to LoS) delay of the multiple propagation paths. Thirdly, since in the blind case the OS is not part of the network infrastructure, its received signal can be more vulnerable to interference and noise. On the other hand, a dedicated OS can be moving which allows the fusion of data measured from different OS positions and hence with different informational content concerning the MS location. It furthermore allows the optimization of OS position regarding the SNR, providing a clear advantage over infrastructure based localization.

Concerning the first point, we assume in this paper that this problem has been solved at the OS carrying an antenna array (see [10]). It is furthermore assumed that the OS is able to separate the multipath components belonging to different MSs, therefore the more realistic multiuser situation can be reduced to the single MS case. That is, the OS provides the estimates of path's direction (DoA) and the relative delay (ToA) which characterize a single MS. In the sequel, we refer to these parameters as "measured multipath parameters." The reader is referred to [11] which describes subspace-based joint space-time filtering and estimation procedures. From field trials in real propagation environments it is well known that measured DoA/ToA parameters are subjected to errors leading to variances of the estimated parameters. Moreover, the chosen model order can be not correct. Overestimation of model order may even create completely wrong results which pretend spurious (or false) paths. This is even aggravated by the nonuniform angular responses of the real antenna arrays because of element coupling and imperfect calibration [11].

If the MS position is calculated from those erroneous multipath parameters, this may result in completely wrong coordinates. However, from the field trials mentioned it is obvious that the multipath parameters that can be clearly attributed to dominant objects in the environment typically sustain over longer parts of the OS track, even if these parameters are slowly changing with time (cf. simulated results in Figures 7 and 8). For example, whereas a path can disappear at some position because of destructive interference, it can show up even stronger at another OS position. Also LoS can occur from time to time depending on the structure of the propagation environment. So, path parameter tracking has the potential to considerably increase the reliability of location estimation results. This leads us to the main contribution of this paper. Just in the spirit of track-before-detect techniques (see [12, 13]), we propose to integrate the information included in the radio channel observations over time by applying the path parameter tracking in the first processing step. In the second step, we accomplish the detection and state estimation of the MS by means of a particle filtering technique using the predefined likelihood function.

The paper is organized as follows. In Section 2, we introduce the localization principle, the underlying measurement model, and the likelihood function. The multipath parameter tracking is introduced in Section 3. In Section 4, we analyze the performance of the localization algorithm in synthetic urban scenarios. Finally, Section 5 summarizes the paper and presents an outlook on our future work.

2. LOCALIZATION PRINCIPLE

For SSL, we are looking for a data model which allows tracing back the geometric information (DoA, relative ToA) to the mobile terminal measured at the single mobile OS. The following considerations reveal the nature of the problem and its solution. Since blind SSL can only measure the relative ToA, information on the LoS distance between OS and MS is lost. If there were pure LoS connection, we could estimate only the looking direction from the OS to the mobile terminal which is insufficient for localizing the MS since the distance is missing. However, if there are multiple delayed impinging paths resulting from reflections at dominant objects in the environment, this would give us additional information since we can trace them back from the OS to the hypothetical MS position. For this purpose, we propose to exploit a priori information about the geometry of the environment from additional sources and process it by means of a RT analysis. Using this approach, it will be possible to

carry out a blind SSL in LoS or even in more difficult NLoS scenarios.

2.1. Wave propagation prediction via 2D ray tracing

In essence, the proposed RT analysis marks the same idea which was already discussed for fingerprint location methods. However, in contrast to the approach in [4], any precalculating and pre-measuring is impossible if the OS is moving. This means that the a priori knowledge about the geometric structure of the environment has to be processed on-the-fly as a part of the localization procedure. For this end, we propose to include a real-time RT model into the blind SSL approach.

In a RT analysis, the propagating radiowaves are modeled by rays following the laws of geometrical optics and uniform theory of diffraction [14]. The RT analysis for radiowave propagation normally consists of two processing steps. In the first step, the search occurs for possible rays radiating from the transmitter position and interacting with obstructions placed in the surrounding area, until finally arriving at the receiver position. In the second step, the electromagnetic parameters of a particular traced ray are calculated regarding the information of its length, the kind of undergone interaction phenomena, and dielectric material properties of involved obstacles. Here we assume equal material properties for all surrounding buildings, while the exact values are unknown. For the sake of computational simplicity we use only 2D terrain data instead of 3D data. Moreover, it may be easier to get 2D data from maps or photos. This should be especially sufficient in case of urban scenarios and the OS on street level. In case of more elaborate scenarios and with available information, the data model can be extended to 3D.

Figure 1 demonstrates a ray tracing example in a simple, synthetic 3D environment and Figure 2 presents its 2D pendant. The circles represent the OS (or receiver) position and MS (or transmitter) position. Hereby, only single bounce scattering (reflection and diffraction) is considered. Note that all but one ray which were found in the 3D environment are also present in a 2D scenario. It is clear that another MS-OS constellation, a different environment, or a higher number of allowed interactions can yield more rays which would be missed in a 2D case. Nevertheless, the rays corresponding to the 2D case will represent a significant subset of the rays detected in the 3D case especially in urban scenarios with OS and MS on the street level. Therefore, it is still possible to solve the localization and tracking problems using a 2D terrain data and radiowave propagation model.

Note that rays which are not considered within 2D-RT analysis would cause a modeling mismatch. In the real measurement applications, this can be avoided by using an antenna array which is able to resolve horizontal and vertical directions of arrival. Then the paths with large vertical DoAs corresponding to the elevated reflectors can be sorted out.

There are two commonly used approaches for the ray search, the launching method and the imaging method [15]. The implemented RT analysis is based on the imaging method. Hereby, the transmitted ray is traced by calculating the imaging point of the transmitter position behind the reflecting surface. Then the imaging point is connected with the receiver position, where the connecting line intersects the reflecting surface in the interaction point. Subsequently, the trace is determined by connecting the transmitter position, interaction point, and receiver position. Note that the single reflection described above follows the law—the angle of incidence equals the angle of reflection. Since the multiple bounce scattering is effectively not a less important propagation phenomenon than a single bounce scattering, we take into account multiple reflections and diffractions as well as their combinations.

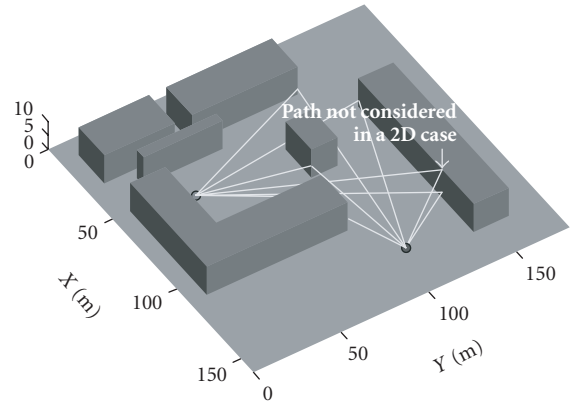

Figure 1: 3D synthetic scenario.

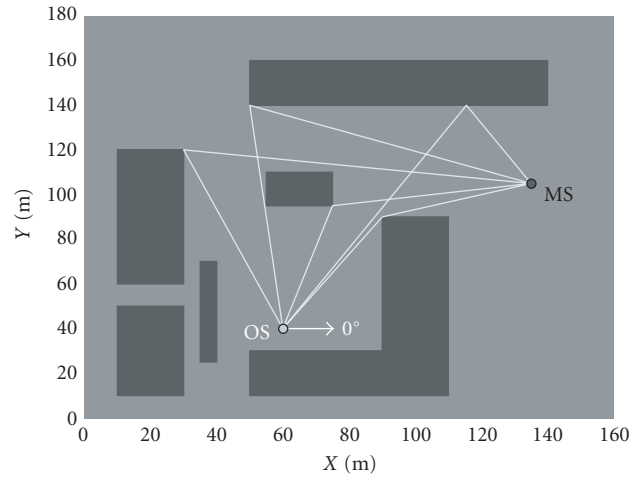

Figure 2: 2D synthetic scenario.

Obviously, the method takes advantage of rich scattering. Multiple bounce reflections allow detection of an MS in NLoS positions even if they are obstructed by multiple obstacles. However, multiple interactions and thus a longer distance also increase path attenuation. Therefore, in the RT model only those rays are considered possessing a minimum signal level at the receiver position. This signal level depends on the sensitivity of the particular measurement system and SNR value. Since we did not specify a particular measurement system, we considered all traced rays in our simulations. The number of traced rays is controlled by the maximum number of bounces.

2.2. Measurement model

In this section, we will introduce the underlying measurement model. In the following discussions, we will suppress the time index whenever there is no danger of ambiguity. Let us denote the set of measured path parameters for a particular time index by

$$\mathbf{z} = \{\mathbf{z}^k\}_{k=1}^{n_K}. \tag{1}$$

n_K is the number of the measured propagation paths which can vary with time. $\mathbf{z}^k$ collects the parameters characterizing the kth measured multipath component and has the following structure:

$$\mathbf{z}^k = \begin{bmatrix} \tau^k & \varphi^k \end{bmatrix}^{\mathbf{T}}. \tag{2}$$

Each multipath component is specified by its relative delay:

$$\tau^k \in [0, \tau_{\max}], \tag{3}$$

with $\tau_{\max}$ denoting the measured delay spread, and by its azimuth direction of arrival:

$$\varphi^k \in [-\pi, \pi]. \tag{4}$$

We denote the known OS position by

$$\mathbf{r} = \begin{bmatrix} \mathbf{x_r} & \mathbf{y_r} \end{bmatrix}^{\mathbf{T}} \tag{5}$$

and the MS position is

$$\mathbf{d} = \begin{bmatrix} \mathbf{x_d} & \mathbf{y_d} \end{bmatrix}^{\mathbf{T}}. \tag{6}$$

Both are allowed to vary with time. In our simulations, we obtained the "measured path parameters" by modeling the radio wave propagation between $\mathbf{r}$ and $\mathbf{d}$ by means of a 2D-RT. The set of modeled path parameters is denoted by

$$\mathbf{h}(\mathbf{r}, \mathbf{d}) = \mathbf{h_d} = \{\mathbf{h}_\mathbf{d}^i\}_{i=1}^{n_T} \tag{7}$$

and represents the parameters which could be measured if there were no disturbing factors due to the measurement process. Note that $\mathbf{h}(\mathbf{r}, \mathbf{d})$ is a nonlinear function since the number of the propagation paths and the values of their parameters depend in a nonlinear way on the position of the MS and OS. Hereby, n_T is the true number of paths at the MS position $\mathbf{d}$. Parameters characterizing the ith true multipath component are contained in a vector:

$$\mathbf{h}_\mathbf{d}^i = \begin{bmatrix} \tau_\mathbf{d}^i & \varphi_\mathbf{d}^i \end{bmatrix}^{\mathbf{T}}, \tag{8}$$

where $\tau_\mathbf{d}^i$ is an excess/relative delay obtained from the originally calculated length of the corresponding ray $l_\mathbf{d}^i$ within the 2D-RT analysis by subtracting the length of the shortest ray in the set and dividing it by the speed of light:

$$\tau_\mathbf{d}^i = \frac{(l_\mathbf{d}^i - \min(\{l_\mathbf{d}^i\}_{i=1}^{n_T}))}{c_{\text{light}}}. \tag{9}$$

```
r = 0
FOR i = 1 : n_T
        u ~ U[0, 1]
        IF u < P_D
                r = r + 1
                m(r) = i
        END IF
END FOR
```

Algorithm 1: Missing paths generation.

```
m = Poi(n_F)
FOR j = 1 : m
        h_FA^j = [ U[0, max({τ_d^i}_{i=1}^{n_T})]  U[−π, π] ]^T
END FOR
h̃_d = h_d^m ⋃ h_FA
```

Algorithm 2: False paths generation.

During the measurement process, the true parameters are affected by different types of errors. Therefore, the measured path parameters are not identical to the true ones $\mathbf{h}(\mathbf{r}, \mathbf{d})$. The low SNR value aggravates the correct separation of the signal and noise space within the eigenvalue decomposition which causes missing detections of the true propagation paths or conversely produces the false paths. Furthermore, we have to consider the measurement uncertainties which distort the true parameter values. The modeling mismatch issue, however, is not considered in this work, that is, we assume that the real measurement environment is perfectly reproduced by the 2D-RT.

We assume that missing detections occur randomly and model it using Algorithm 1. Hereby, P_D is the detection probability of the multipath components, for example, $P_D = 0.8$ means that 80% of the true paths were correctly detected. With $u \sim U[0, 1]$, we describe the realization of the uniform distribution $U[0, 1]$, hereby 0 and 1 are the interval limits. Vector $\mathbf{m}$ comprises the indices of the detected propagation paths and the set of detected path parameters is a subset of $\mathbf{h_d}$ and is denoted by $\mathbf{h}_\mathbf{d}^\mathbf{m}$.

The generation of the false propagation paths is a random process as well. We model the number of false paths (also referred to as spurious paths, false alarms or clutter) m as a Poisson-distributed random variable with the mean number of false alarms n_F (see Algorithm 2). Since the false paths originate from the noise space within the eigenvalue decomposition, their parameters are uniformly distributed in the delay and DoA domain. $\tilde{\mathbf{h}}_\mathbf{d}$ consists of the incomplete set of true paths and the set of false paths. Finally, we extend the measurement model to additive measurement noise and yield the following measurement equation:

$$\mathbf{z} = \{\tilde{\mathbf{h}}_\mathbf{d}^k + \mathbf{w}^k\}_{k=1}^{n_K}. \tag{10}$$

$\mathbf{w}^k$ denotes the measurement noise with entries:

$$\mathbf{w}^k = \begin{bmatrix} w_\tau^k & w_\varphi^k \end{bmatrix}^{\mathrm{T}}, \tag{11}$$

where $w_\tau^k \sim \mathcal{N}(0, \sigma_{\tau_k}^2)$ and $w_\varphi^k \sim \mathcal{N}(0, \sigma_{\varphi_k}^2)$ are the realizations from Gaussian distributions. Let $\sigma_{\tau_k}^2, \sigma_{\varphi_k}^2$ denote the noise variances and let

$$\mathbf{C}^k = \mathrm{diag}(\sigma_{\tau_k}^2, \sigma_{\varphi_k}^2) \tag{12}$$

denote the noise covariance matrix of the kth measured path. The values of the noise variances depend on the array configuration, system bandwidth, SNR, and are typically different for every measured propagation path. For simplicity, we assume equal variances for all paths. The measurement model is now complete. In the next section, we define the underlying likelihood function.

2.3. Data association and likelihood function

The definition of the likelihood function is one of the central points of the proposed localization procedure. The likelihood function provides a measure of proximity between the multipath parameters predicted by the 2D-RT analysis for an arbitrary MS position and the measured multipath parameters obtained by the antenna array at the OS. In calculating the match between the modeled and measured path parameters, we consider the types of error which distort the path parameters and those which either cause missing detections of multipath components or produce the false ones. This leads to a combinatorial association problem [16, 17] since there are many ways to interpret the measured data. Since we have no a priori information about the location of the MS, the straightforward strategy is to sample the region of interest. Let us assume a sampled, hypothetical MS position specified by two Cartesian coordinates:

$$\mathbf{s}_p = \begin{bmatrix} x_p & y_p \end{bmatrix}^{\mathbf{T}}. \tag{13}$$

In total, let there be P hypothetical MS positions with $p = 1, \ldots, P$ which can be randomly chosen or arranged in a grid. P is thus a design parameter of the localization algorithm to be chosen appropriately depending on the size and the density of the environmental scenario. We model the radiowave propagation between the known OS position $\mathbf{r}$ and $\mathbf{s}_p$ by means of 2D-RT analysis in the same manner as in (7). The set of predicted path parameters is denoted by

$$\mathbf{h}(\mathbf{r}, \mathbf{s}_p) = \mathbf{h}_{\mathbf{s}_p} = \{\mathbf{h}_{\mathbf{s}_p}^i\}_{i=1}^{n_T} \tag{14}$$

representing the pendant to the measured parameters defined in (10). Hereby, n_P is the number of the predicted propagation paths at the hypothetical MS position $\mathbf{s}_p$. Parameters characterizing the ith predicted multipath component are contained in a vector:

$$\mathbf{h}_p^i = \begin{bmatrix} \tau_p^i & \varphi_p^i \end{bmatrix}^{\mathbf{T}}. \tag{15}$$

Note, that only those paths are considered whose excess delays lie within the measured delay spread $\tau_{\max}$ defined in (3), that is, $\{\tau_p^i\}_{i=1}^{n_p} \leq \tau_{\max}$.

We denote the likelihood function by $p(\mathbf{z} \mid \mathbf{s}_p)$ which is a conditional probability density and though can be written as a sum over all possible data interpretations according to the total probability theorem:

$$\begin{aligned} p(\mathbf{z} \mid \mathbf{s}_p) &= \sum_{E_{i_1 \cdots i_{n_p}}} p(\mathbf{z}, E_{i_1 \cdots i_{n_p}} \mid \mathbf{s}_p) \\ &= \sum_{i_1=0}^{n_K} \cdots \sum_{i_{n_p}=0}^{n_K} p(\mathbf{z} \mid E_{i_1 \cdots i_{n_p}}, \mathbf{s}_p)\, p(E_{i_1 \cdots i_{n_p}} \mid \mathbf{s}_p). \end{aligned} \tag{16}$$

We denote a possible data interpretation by $E_{i_1,\ldots,i_{n_p}}$, where $i_1 \cdots i_j \cdots i_{n_p}$ is an association vector of modeled to measured propagation paths, with

$$i_j = \begin{cases} 0, & \text{no association, path is not} \\ & \text{detected or is due to clutter} \\ k \in \{1, \ldots, n_K\}, & j\text{-th predected path is associated} \\ & \text{with the } k\text{-th measured path.} \end{cases} \tag{17}$$

Note that one measured path can be associated only with one predicted path. Since the number of measured and predicted paths can differ, there can be several not associated paths. For example, E_{0210} represents a possible data interpretation which means that $n_p = 4$, that is, there are 4 predicted propagation paths. Furthermore, the first and the fourth predicted path were not associated; the second predicted path was associated with the second and the third predicted paths with the first measured path. Let us elaborate on the terms from (16). Under the assumption that the measured propagation paths are independent of each other, we obtain a factorized likelihood model conditioned on an association hypothesis $E_{i_1,\ldots,i_{n_p}}$ (see [17]):

$$\begin{aligned} p(\mathbf{z} \mid E_{i_1 \cdots i_{n_p}}, \mathbf{s}_p) &= \prod_{k=1}^{n_K} p(\mathbf{z}^k \mid E_{i_1 \cdots i_{n_p}}, \mathbf{s}_p) \\ &= \prod_{j \in I_0} p_C(\mathbf{z}^{i_j}) \cdot \prod_{j \in I} p_A(\mathbf{z}^{i_j} \mid \mathbf{h}_p^j), \end{aligned} \tag{18}$$

where $I = \{j \in \{1, \ldots, n_p\} \wedge i_j \neq 0\}$ is the subset of n indices corresponding to the predicted paths which are associated with the measured paths and $I_0 = \{j \in \{1, \ldots, n_p\} \wedge i_j = 0\}$ is a subset of $n_K - n$ not associated paths. In the above, $p_C(\mathbf{z}^{i_j})$ denotes the clutter likelihood model for the i_jth measured path which is assumed to be uniform over the field of view of the sensor referred to as $|\mathrm{FoV}| = 2\pi\tau_{\max}$. $p_A(\mathbf{z}^{i_j} \mid \mathbf{h}_p^j)$ denotes the association likelihood for an i_jth measured path associated with the jth predicted path. Since the measurement noise is assumed to be independent and Gaussian (see (12)), the likelihood for the i_jth measured multipath component, under the hypothesis that it is associated with the jth predicted path, is given by

$$p_A(\mathbf{z}^{i_j} \mid \mathbf{h}_p^j) = \mathcal{N}(\mathbf{h}_p^j; \mathbf{z}^{i_j}, \mathbf{C}^{i_j}). \tag{19}$$

Following the assumptions made above, the expression (18) simplifies to

$$p(\mathbf{z} \mid E_{i_1 \cdots i_{n_p}}, \mathbf{s}_p) = |\mathrm{FoV}|^{-(n_K - n)} \cdot \prod_{j \in I} \mathcal{N}\left(\mathbf{h}_p^j; \mathbf{z}^{i_j}, \mathbf{C}^{i_j}\right). \quad (20)$$

The second factor in (16) $p(E_{i_1 \cdots i_{n_p}} \mid \mathbf{s}_p)$ is referred to as association prior (see [17]). We assume the prior of the association hypothesis to be independent of the state and past values of the association hypothesis and thus can be expressed as a product of

$$p(E_{i_1 \cdots i_{n_p}} \mid \mathbf{s}_p) = p(i_1 \cdots i_{n_p} \mid n, n_K, n_p)\, p_F(n_K - n)\, p(n \mid n_p)\, p(n_p). \quad (21)$$

Hereby, the first term describes the probability of a single hypothesis under the assumption that all hypotheses are equivalent and is given as

$$p(i_1 \cdots i_{n_p} \mid n, n_K) = (N_H)^{-1} = \left(\binom{n_p}{n} \cdot \frac{n_K!}{(n_K - n)!} \right)^{-1}. \quad (22)$$

N_H is the number of valid hypotheses which follows from the number of ways of choosing a subset of n elements from the available predicted propagation paths n_p multiplied by the number of possible associations between associated n and measured n_K paths. Note that n_p is a hypothetical value of the true number of measured paths n_T, which is normally unknown. Since we have no a priori information about n_T, we assume a uniform prior for all values of n_P:

$$p(n_p) = \frac{1}{\max\left(\{n_p\}_{p=1}^{P}\right) + 1}. \quad (23)$$

The second term in (21) expresses the probability of $n_K - n$ false alarms:

$$p_F(n_K - n) = \frac{(n_F)^{(n_K - n)}}{(n_K - n)!} \cdot \mathrm{e}^{-n_F} \quad (24)$$

which is assumed to follow a Poisson distribution with rate parameter n_F. Finally, the third factor in (21) denotes the probability of n associated paths which is assumed to follow the binomial distribution:

$$p(n \mid n_p) = \binom{n_p}{n} P_D^n (1 - P_D)^{(n_p - n)} \quad (25)$$

incorporating all possible ways to group n paths among n_p assumed true measurements. All measured propagation paths share the same known detection probability P_D according to the measurement model introduced in Section 2.2. Under the assumptions discussed above, the likelihood function can be expressed as

$$p(\mathbf{z} \mid \mathbf{s}_p) \propto \sum_{E_{i_1 \cdots i_{n_p}}} \frac{(n_F |\mathrm{FoV}|)^{(n_K - n)} P_D^n \cdot \prod_{j \in I} \mathcal{N}\left(\mathbf{h}_p^j; \mathbf{z}^{i_j}, \mathbf{C}^{i_j}\right)}{\mathrm{e}^{n_F} n_K! (1 - P_D)^{(n - n_p)}}. \quad (26)$$

Table 1: Valid hypothesis after gating.

0 association	1 association	2 associations	3 associations
E_{00000}	E_{10000}	E_{10300}	E_{10305}
—	E_{00300}	E_{10400}	E_{10405}
—	E_{00400}	E_{10005}	—
—	E_{00005}	E_{00305}	—
—	—	E_{00405}	—

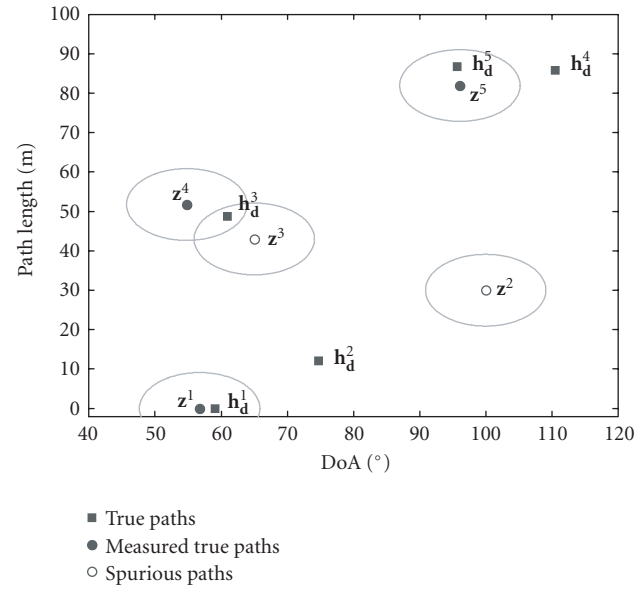

Figure 3: Paths mapped into the measurement space.

The number of possible associations N_H within the introduced likelihood function can be enormous. It increases exponentially with the number of measured and predicted paths. Therefore, suitable techniques for the complexity reduction are crucial.

2.4. Gating

Gating is one of the strategies for reducing computational complexity. Hereby a validation region is defined for each measured propagation path. Only those predicted paths which fall within the validation region are allowed to be associated with the particular measured path.

In the following, we present a gating procedure which is applied within the proposed localization technique. Figure 3 demonstrates graphically an example of measured and predicted paths mapped into the measurement space corresponding to the MS-OS constellation of Figure 2. The measured paths are depicted by circles and their validation regions as ellipses. The filled circles represent the true measured multipath components whereas the white circles represent the false paths. The set of the true paths is depicted by squares. We assumed a situation with two missing and two false paths.

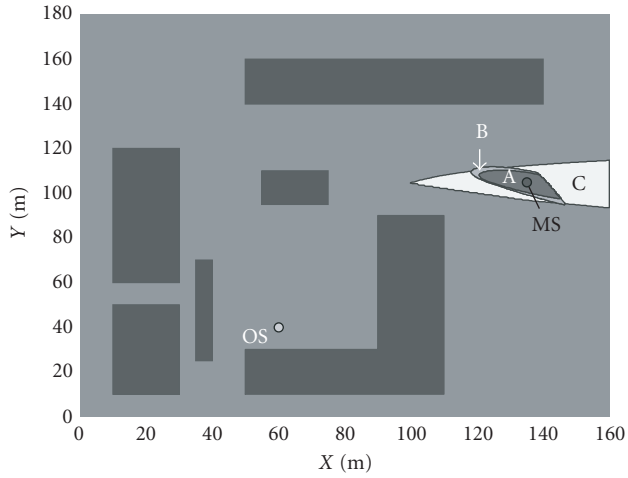

Figure 4: Region A corresponds to the ideal case with no false and no missing paths; region B, 5th path is missed; region C, 3rd path is missed.

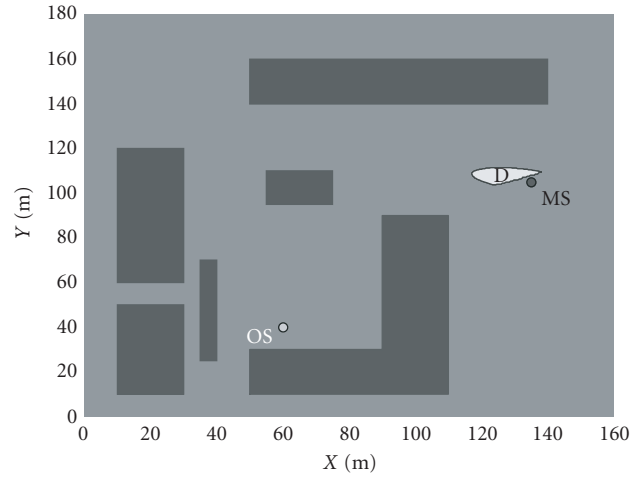

Figure 5: Region D corresponds to the case with one false and no missing paths.

We introduce the normalized squared distance between the kth measured and ith predicted path based on measurement uncertainties:

$$d^{k,i} = \left(\mathbf{z}^k - \mathbf{h}_{\mathbf{d}}^i\right)^{\mathrm{T}} \left(\mathbf{C}^k\right)^{-1} \left(\mathbf{z}^k - \mathbf{h}_{\mathbf{d}}^i\right). \tag{27}$$

Since the measurement noise is assumed to be Gaussian, $d^{k,i}$ is chi-square distributed with the 2 degrees of freedom which is equal to the dimension of $\mathbf{z}^k$. ε denotes the parameter determining the boundaries of the validation region. The validation region is an ellipsoid that contains a given probability mass. For example, $\varepsilon = \chi^2_{2;0.99}$ means that the corresponding validation region contains 99% of probability mass. The association between the kth measured and ith predicted propagation path is valid if $d^{k,i} \leq \varepsilon$. This condition decreases the number of possible hypotheses significantly. Applying this pruning strategy to the example from the Figure 3, we obtain the following hypotheses sorted according to the number of achieved associations between the measured and predicted paths.

E_{00000} is the null hypothesis which considers the case that all measured paths are false alarms. Note that Table 1 contains 12 valid hypotheses which contain the major likelihood weight. An exhaustive calculation would require the consideration of 1546 hypotheses according to (22). However, the contribution of most of them is negligible and can be ignored.

2.5. Impact of missing and false paths on the positioning accuracy

In this section, we demonstrate with a simple example, how missing and false propagation paths affect the localization result. Therefore, we use the already known MS-OS constellation from Figure 2. Remember that the true parameters depicted by squares are represented in Figure 3. We consider three different cases and calculate the likelihood function using a grid of 0.5 m for each case. Figure 4 presents three regions corresponding to the three cases which contain ca. 95% of the whole probability mass of the respective likelihood function. Hereby, region A corresponds to the ideal case with no spurious paths and no missing true paths. Region B corresponds to the situation, where $\mathbf{h}_{\mathbf{d}}^5$, the 5th true path, is missed, and for region C we assumed that the 3rd true path $\mathbf{h}_{\mathbf{d}}^3$ is missed. Furthermore, we assumed $P_D = 0.8$, $n_F = 1$ and a measurement noise covariance of $\mathbf{C}_t = \mathrm{diag}((3\,\mathrm{m}/c_{\mathrm{Light}})^2, (3^\circ)^2)$. However, we do not add measurement noise and false paths since we want to test the impact of nondetection alone.

We observe that the true MS position is included in all of these regions. Furthermore, we observe the enlarging of the uncertainty regions in case B and C compared to case A. Note, furthermore, that whereas the difference between case A and B is marginal, it is more significant between cases A and C. It means that missing true paths in general leads to a poor positioning accuracy. However, the impact of different missed paths can be different. This behavior can be explained as follows. In the set of propagation paths corresponding to the particular position some of the paths characterize this position in a distinctive way since they can be received only from this position. If these paths are not detected, for example, due to measurement disturbances, the positioning uncertainty will increase significantly, like in case C. On the other hand, there are propagation paths whose parameters are related to other MS positions as well. Therefore, we obtain negligible deterioration of positioning accuracy if they are missed, like in case B.

Now, we attend to the case D depicted in Figure 5. Here we assumed no missing paths and one false propagation path with parameters $[28\,\mathrm{m} \quad 124^\circ]^{\mathrm{T}}$. Note that region D containing ca. 95% of the likelihood weight does not include the true MS position. That is, although all paths were correctly detected, the position estimation results in wrong coordinates due to the single spurious path.

In the next section, we propose a technique which mitigates the impact of missing and false paths on the positioning accuracy.

Initialization
$t = 1; c = 0; \hat{\mathbf{g}}_t^k = [\mathbf{z}_t^k(1)\ \mathbf{0}\ \mathbf{z}_t^k(2)\ \mathbf{0}]^{\mathbf{T}}; \mathbf{P}_t^k = \mathbf{P}_{\text{Init}}$
WHILE $t < T_p$
  $t = t + 1$
  $[\mathbf{y}, \mathbf{Y}]$ = Association $[\hat{\mathbf{g}}_{t-1}^k, \mathbf{P}_{t-1}^k, \mathbf{z}_t, \mathbf{C}_t]$
  IF $\mathbf{y} \neq [\,] \& \mathbf{Y} \neq [\,]$
    $c = 0$
  ELSE
    $c = c + 1$
  END IF
  IF $c < M$
    $[\hat{\mathbf{g}}_t^k, \mathbf{P}_t^k] = KF\text{-path}\ [\hat{\mathbf{g}}_{t-1}^k, \mathbf{P}_{t-1}^k, \mathbf{y}, \mathbf{Y}]$
  ELSE
    $t = T_p$
  END IF
END WHILE

Algorithm 3: Path parameter tracking procedure.

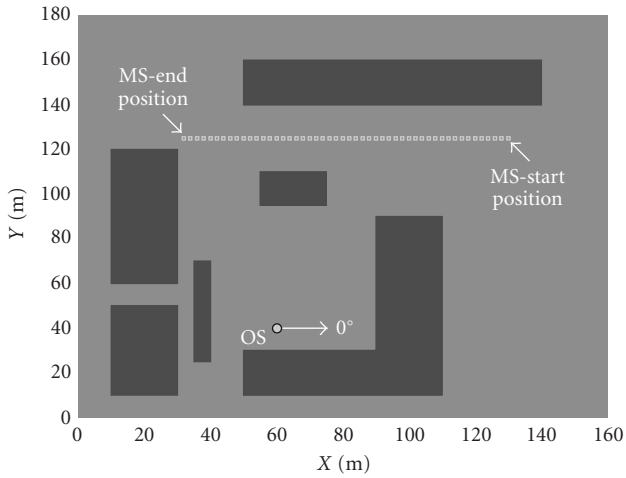

Figure 6: 2D synthetic scenario with MS trajectory.

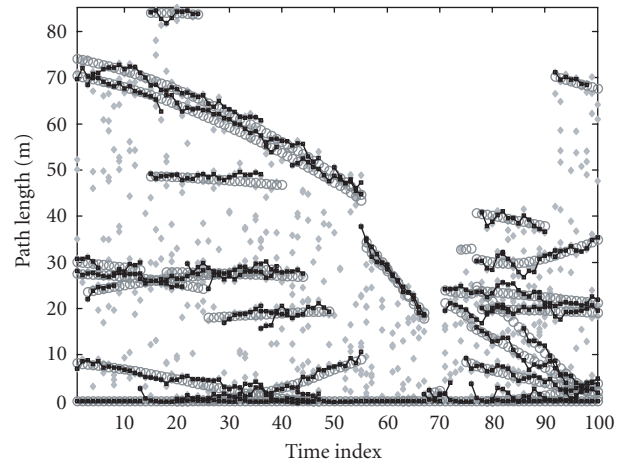

Figure 7: Relative path lengths: light dots represent measurement; black tracks represent the tracking result; circles represent the true values.

3. MULTIPATH PARAMETER TRACKING FOR LOCALIZATION

The simulations have shown that missing propagation paths as well as the presence of false paths can severely degrade the positioning accuracy. For example, the spurious paths produce more association hypotheses and obviously results in a higher likelihood value for the incorrect hypothetical MS positions. On the other hand, due to the incomplete set of true parameters contained in the measured path set, the highest likelihood value can be achieved at the incorrect hypothetical MS position if its predicted paths fit better with the observation. In order to make the assumptions about the true and spurious propagation paths more precise, we propose to use a priori information included in the temporal behavior of the mobile radio channel. In [18], investigation results on the estimation of the varying space-time structure of the mobile radio channel in the context of multidimensional channel modeling [19] are presented. The underlying measurements were carried out by means of a real-time channel sounder [20] which delivers instantaneous radio channel observations referred to as snapshots. From each of these snapshots, a set of multipath parameters is estimated. It was observed that the straightforward assumption about temporal independency of subsequent snapshot estimates is not correct. On the contrary, it was found out that the specular part of the channel response contains wave propagation paths which persist along a limited number of snapshots. A maximum likelihood batch estimation procedure for the tracking of multipath parameters was implemented and verified on measured data. The insight gained into the mobile radio channel modeling can be directly applied to the purpose of localization. We propose to use the multipath tracking procedure in order to evaluate the reliability of the measured propagation paths. The false paths possess a random occurrence character and do not persist during the observation period of few measurements in contrast to the true paths which parameters vary deterministically depending on the dynamics of the MS and OS. It is desirable to detect the false paths and to exclude them from the localization process since they deteriorate the position estimation. On the other hand it is important to detect and to maintain the tracks of the true paths. In the following we will try to satisfy these requirements by applying a tracking technique to the sequence of measurements.

3.1. Multipath parameter tracking procedure

We propose to use a parallel bank of linear Kalman filters for tracking the measured paths. In situations with closely spaced parameters corresponding to different paths, we apply a nearest neighbor principle [21]. Although the following example demonstrates the procedure in case of a single path, it can easily be extended to a number of paths. Let us denote the state variable of the kth propagation path at time t by

$$\mathbf{g}_t^k = \left[\tau\ \ \dot{\tau}\ \ \varphi\ \ \dot{\varphi}\right]^{\mathbf{T}}. \tag{28}$$

Hereby, $\dot{\tau}$ and $\dot{\varphi}$ describe the mean variation rate of the excess delay and direction of arrival, respectively. The transition matrix is defined by

$$\Phi = \begin{bmatrix} \mathbf{F} & \mathbf{0}^{2\times 2} \\ \mathbf{0}^{2\times 2} & \mathbf{F} \end{bmatrix}, \tag{29}$$

where $\mathbf{0}^{2\times 2}$ is a 2×2 zero matrix and

$$\mathbf{F} = \begin{bmatrix} 1 & T \\ 0 & 1 \end{bmatrix}, \tag{30}$$

with a time interval T. The state equation can be written as

$$\mathbf{g}_t^k = \Phi \cdot \mathbf{g}_{t-1}^k + \mathbf{v}_{t-1}^k, \tag{31}$$

where

$$\mathbf{v}_{t-1}^k = \begin{bmatrix} \frac{T^2}{2} \nu_{\dot{\tau},t-1} & T\nu_{\dot{\tau},t-1} & \frac{T^2}{2} \nu_{\dot{\varphi},t-1} & T\nu_{\dot{\varphi},t-1} \end{bmatrix}^{\mathrm{T}} \tag{32}$$

is the process noise according to [22], with $\nu_{\dot{\tau}} \sim \mathcal{N}(0, \sigma_{\dot{\tau}}^2)$ and $\nu_{\dot{\varphi}} \sim \mathcal{N}(0, \sigma_{\dot{\varphi}}^2)$. Hereby, $\sigma_{\dot{\tau}}$ and $\sigma_{\dot{\varphi}}$ specify the nonlinearities in the variation rate of excess delay and direction of arrival, respectively. Their values can be roughly estimated from the highest expected velocity of the MS and OS. With (32), we can define the covariance matrix of the process noise:

$$\mathbf{Q} = \mathrm{E}[\mathbf{v}_{t-1}^k \cdot (\mathbf{v}_{t-1}^k)^{\mathrm{T}}], \tag{33}$$

with $\mathrm{E}[\cdot]$ denoting the expectation operator. For simplicity, $\mathbf{Q}$ is assumed to be constant and equal for all paths and points in time. The measured parameters of the particular path labeled with the time index are related to the state of the path via the linear measurement equation:

$$\mathbf{z}_t^k = \begin{bmatrix} 1 & 0 & 0 & 0 \\ 0 & 0 & 1 & 0 \end{bmatrix} \cdot \mathbf{g}_t^k + \mathbf{w}_t^k = \mathbf{H}\mathbf{g}_t^k + \mathbf{w}_t^k, \tag{34}$$

in accordance with the measurement model (10), (11), and (2). A pseudocode description of a single cycle of the multipath tracking procedure is presented in Algorithm 3.

The input data consists of path parameters measured at T_p points in time and the corresponding covariance matrices. The output contains the sequence of state estimates of a single path with the corresponding covariance matrices. The path track is initialized by the kth measured path and initial state covariance matrix $\mathbf{P}_{\mathrm{Init}}$. There are n_K measured paths at each point in time, however, only one measurement can be associated with the predicted state estimate. We propose to use the nearest neighbor principle in order to choose the most suitable candidate. The corresponding pseudocode can be found in Appendix A.1. The output of the association procedure $\mathbf{y}$ and $\mathbf{Y}$ denotes the associated measured path and its covariance matrix. $\mathbf{y}$ and $\mathbf{Y}$ are empty ($\mathbf{y} = [\,]$, $\mathbf{Y} = [\,]$), if no association could be achieved. In this case, the subsequent Kalman filter proceeds without filtering step (see for details in Appendix A.2). Furthermore, the counter c which collects the number of nonassociations within the recent M points in time is increased by one. As soon as c achieves M, the track is declared to be finished. This functionality allows to bridge over the gaps in the track caused by the missing detections of the true paths. Moreover, it enables to detect the false paths which normally can not be continued.

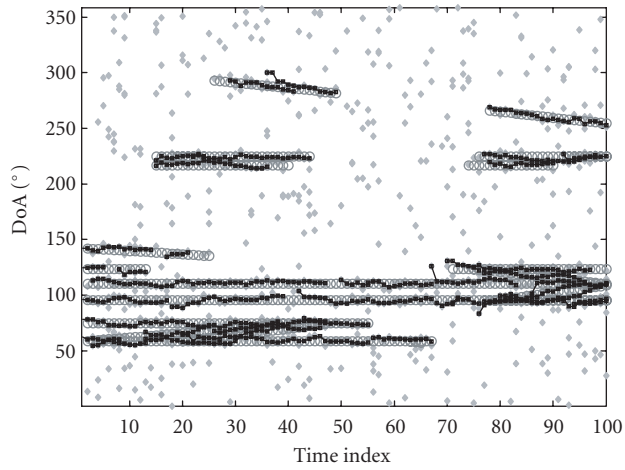

Figure 8: DoAs: light dots represent measurement; black tracks represent the tracking result; circles represent the true values.

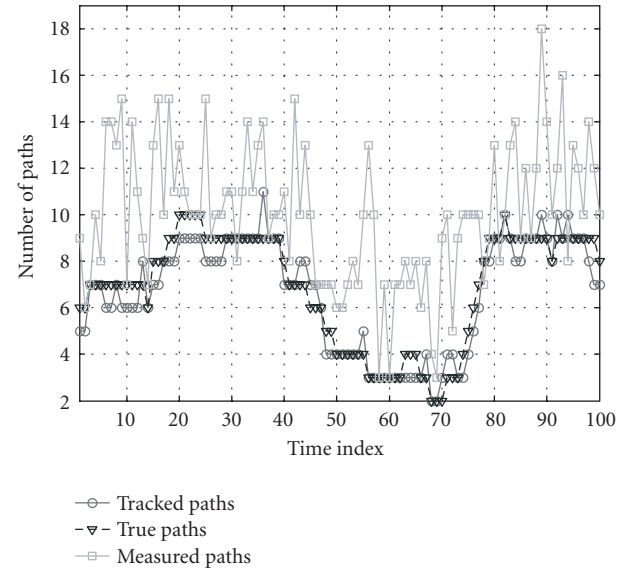

Figure 9: Number of tracked, true, and measured multipath components.

For the sake of simplicity, the functionality of the demonstrated procedure was limited to the tracking of a single path. It can be extended to tracking of a number of paths. In the next section, we present the simulation results of the proposed path tracking algorithm.

3.2. *Simulation results for multipath parameter tracking*

Figure 6 presents the synthetic 2D scenario used for simulations. We assumed a static OS and an MS moving along the depicted straight trajectory. The number of observations

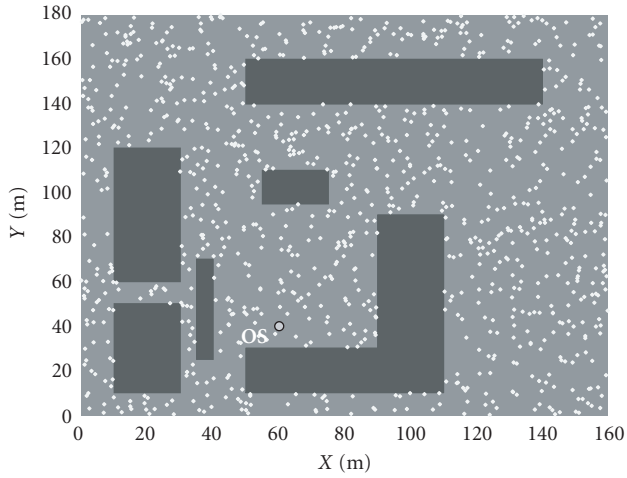

Figure 10: Initial particle distribution.

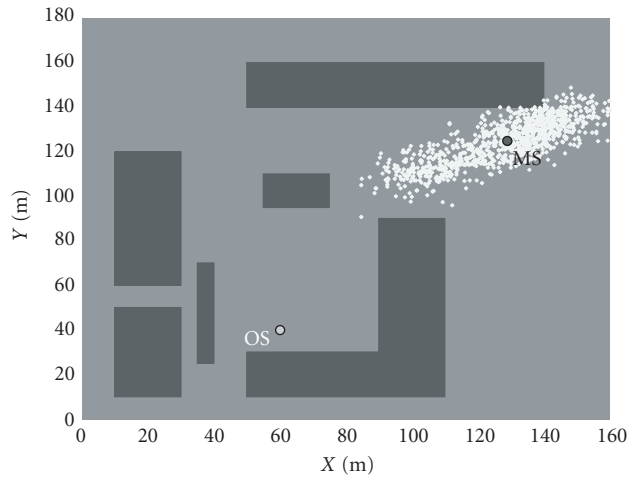

Figure 11: Case 1: particle distribution after the first SIR cycle.

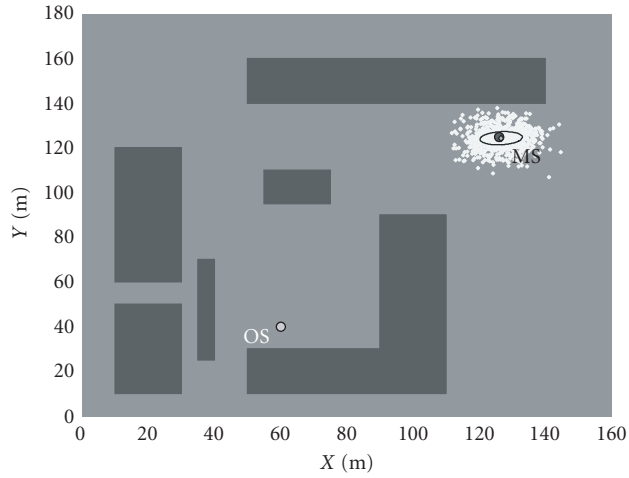

Figure 12: Case 1: Initialization result achieved after the fifth SIR cycle.

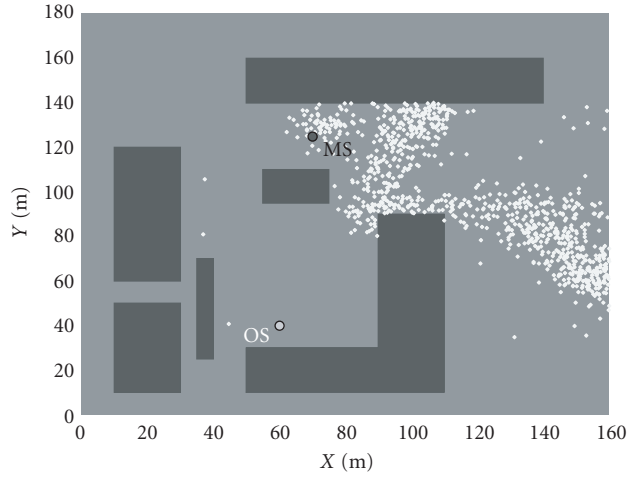

Figure 13: Case 2: particle distribution after the first SIR cycle.

T_p was set to 100. The measurement noise covariance was set to $\mathbf{C}_t^k = \text{diag}((1\text{m}/c_{\text{Light}})^2, (3^\circ)^2)$ and is assumed to be equal for all paths and points in time. Furthermore, we assumed $P_D = 0.8$ and $n_F = 4$. We generated the measurement using the model explained in Section 2.2. Hereby, we assumed a single bounce scattering for these simulations. Figure 7 presents the relative path lengths and Figure 8 the DoAs against time. In spite of the disturbances due to the measurement noise, and nondetection process, the estimated parameters almost match the true ones. This can be also observed in Figure 9 which shows the number of the tracked, true, and measured paths over time depending on the changing environment.

4. EXPERIMENTS AND RESULTS

In this section, we present the simulation results of the proposed space state initialization technique for the blind MS tracking. We use the synthetic scenario represented in Section 3.2. We will try to initiate the track at different parts of the trajectory depicted in Figure 6 in order to evaluate the performance of the algorithm under different environmental conditions. Moreover, it is informative to observe the dependency of the positioning result from the true number of propagation paths which can be seen from Figure 9. In the first case, we assumed an NLoS MS position "round the corner," it is given by $[130\,\text{m}\ \ 125\,\text{m}]^{\text{T}}$. In the second case, we also chose an NLoS position at $[71\,\text{m}\ \ 125\,\text{m}]^{\text{T}}$ which is obstructed by a building. The third case demonstrates a LoS position at $[41\text{m}\ \ 125\,\text{m}]^{\text{T}}$. The velocity vector $[-1\,\text{m/s}\ \ 0\,\text{m/s}]^{\text{T}}$ corresponding to a pedestrian velocity is equal in all three cases. The measurement noise covariance was set to $\mathbf{C}_t^k = \text{diag}((3\,\text{m}/c_{\text{Light}})^2, (5^\circ)^2)$. Furthermore, we assumed $P_D = 0.8$ and $n_F = 4$. We have applied a sampling importance resampling (SIR) filter, a well-known particle filtering technique (see [13, 23]), for the MS position initialization. Within the SIR procedure, we used the proposed

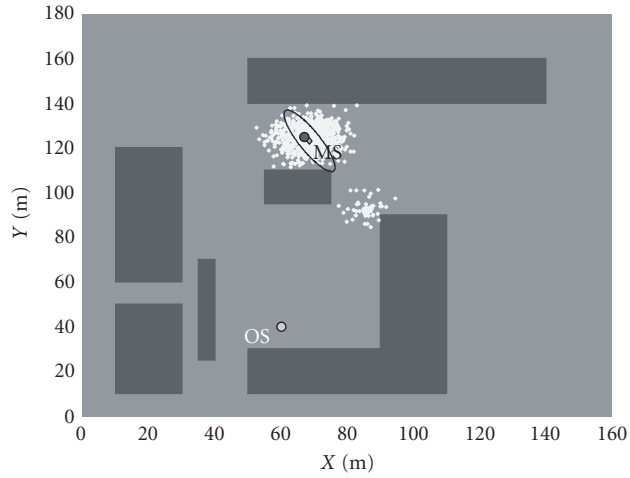

Figure 14: Case 2: Initialization result achieved after the fifth SIR cycle.

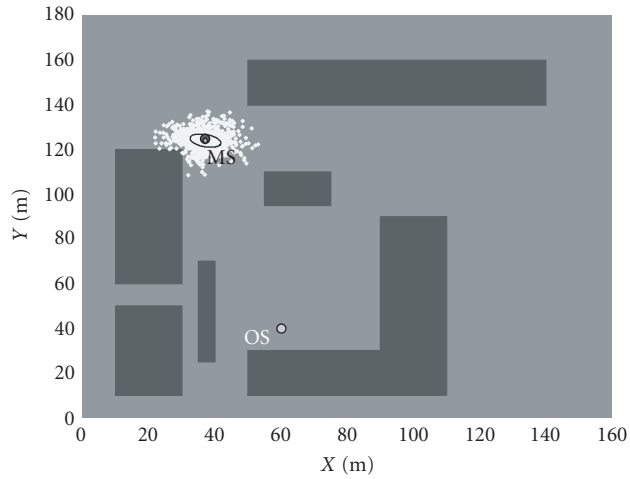

Figure 15: Case 3: Initialization result achieved after the fifth SIR cycle.

likelihood function with preceding path parameter tracking. The pseudocode of the SIR filter and the flow chart of the whole initialization algorithm are presented in Appendices A.3 and A.4, respectively.

The following rough assumptions concerning the initial MS state were considered within the SIR algorithm. The MS is located somewhere outdoor in the region of interest depicted in Figure 10, that is, the location probaibility is equal for all outdoor positions. Hence, we model the initial position uncertainty as a uniform distribution in the region of interest except for the indoor areas. We assume the measurement rates of at least 1 observation per second, that is, the state variation of the MS moving with the maximum velocity of up to 5 km/h (valid for pedestrian area) is negligible. Therefore, we limit the MS state to the x and y coordinates only and define the following state dynamics function:

$$\mathbf{s}_{p,t} = \mathbf{I} \cdot \mathbf{s}_{p,t-1} + \boldsymbol{\omega}_{p,t-1}, \tag{35}$$

where $\mathbf{s}_{p,t}$ denotes the sampled MS position p at time t, specified in (13) also referred to as a particle. $\mathbf{I}$ is a 2×2 identity matrix and $\boldsymbol{\omega}_{p,t-1}$ is a process noise with the entries $\boldsymbol{\omega}_{p,t-1} = [\omega_x \ \ \omega_y]^{\mathrm{T}}$ which are modeled as realizations from Gaussian distributions $\omega_x \sim \mathcal{N}(0, \sigma_x^2)$ and $\omega_y \sim \mathcal{N}(0, \sigma_y^2)$. In our example, σ_x and σ_y were set to 5 m. The measurement equation is given by (10) and the likelihood function available for pointwise evaluation is defined in (26). That is, the assumptions required to use the SIR are satisfied (see [13]). Figure 10 shows 1000 samples randomly chosen from the region of interest which approximate the initial position uncertainty. During the first cycle of the SIR algorithm, the likelihood weight is evaluated for every particle. The subsequent resampling step eliminates particles with low likelihood weights and multiplies particles with high likelihood weights. Figure 11 presents the particle distribution for the first case after the resampling in the first cycle of the SIR filter. Note how the particles are crowded around the true MS position depicted by a black circle. After the fifth SIR cycle, we obtained a distribution shown in Figure 12 and stopped the filtering. The estimated position depicted by light point lies very close to the true MS position. The ellipse indicates the 3σ region of the estimated state covariance matrix.

The second case is the most difficult one. Figure 13 shows the wide distribution of particles after the first SIR cycle. Only few of them are close to the true MS position. This behavior is caused by the fact that there are only 3 true propagation paths at this MS position (see Figure 9, time index 60). Therefore, we achieve inferior position accuracy compared to the first case (see Figure 14).

Figure 15 presents the initialization result for the third case achieved after the fifth SIR cycle. Note that the 3σ ellipse is the smallest in this case. This is due to the highest number of propagation paths corresponding to this MS position (see Figure 9, time index 90).The simulations were carried out in MATLAB. For a single cycle of the algorithm, we needed ca. 3 minutes using a 3 GHz PC.

5. CONCLUSION

We presented a track-before-detect method for initialization of blind mobile terminal tracking in urban scenarios. The key role plays, hereby, the proposed likelihood function which determines the proximity of the measured and predicted multipath components with respect to all possible association hypotheses between them. The measurements of the multipath components are provided by an OS equipped with an antenna array. The predicted temporal and spatial structure of the multipath components is generated by means of the 2D-RT analysis using a priori information about the location of the scattering objects.

In order to mitigate the impact of missing and false propagation paths on the positioning result, we proposed the preprocessing of the measured path parameters by means of a linear Kalman filter.

The likelihood function which is algorithmically defined for a randomly distributed set of potential MS positions was applied within the particle filtering technique and was tested in the synthetic environment. The simulation results showed

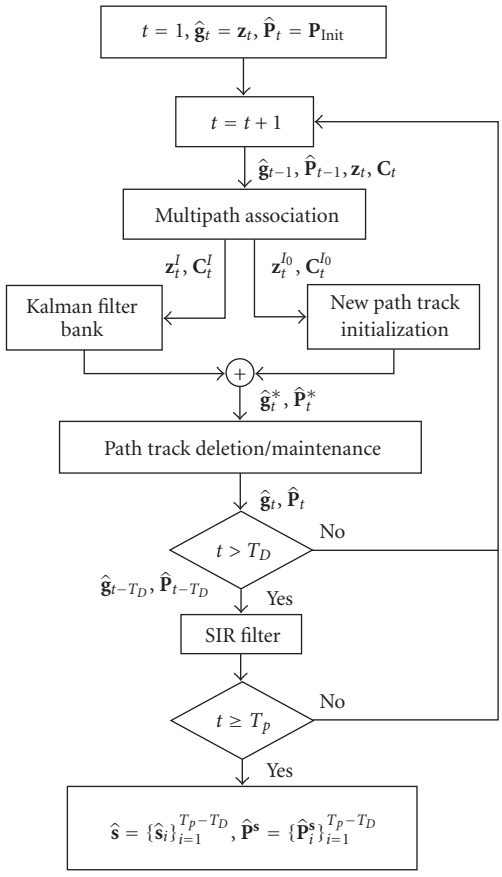

Figure 16: Flow chart of the proposed state space initialization technique.

that the proposed track-before-detect technique provides a robust and accurate state initiation which is essential for the subsequent track maintenance part of the MS tracking algorithm. This, however, is the subject of our future work.

APPENDIX

A.1. Association procedure

Algorithm 4 shows the association procedure used within the tracking of multipath parameters. Hereby, $\hat{\mathbf{g}}_{t-1}$ and $\mathbf{P}_{t-1}$ denote the state estimate and state covariance of the previous point in time. μ is a state prediction and $\mathbf{S}^k$ is the measured innovations covariance. d^k denotes the squared distance based on the measurement innovations for the kth measured path and ε denotes the validation region. A measured path with the smallest squared distance d^j lying within the validation region is assumed to be the most suitable candidate for the association with $\hat{\mathbf{g}}_{t-1}$.

A.2. Kalman filter for multipath parameter tracking

The Kalman filter equations presented in Algorithm 5 belong to the standard procedure and can be found in [13, 21]. If there is no measurement at the current point in time t available, the predicted state $\mathbf{g}_t$ from (31) is taken without filtering step.

$$
\begin{aligned}
&[\mathbf{y}, \mathbf{Y}] = \text{Association}\left[\hat{\mathbf{g}}_{t-1}, \mathbf{P}_{t-1}, \{\mathbf{z}_t^k\}_{k=1}^{n_k}, \{\mathbf{C}_t^k\}_{k=1}^{n_k}\right]\\
&\quad \mu = \Phi \cdot \hat{\mathbf{g}}_{t-1}\\
&\quad \text{FOR } k = 1 : n_k\\
&\qquad \mathbf{S}^k = \mathbf{H}(\Phi \cdot \mathbf{P}_{t-1} \cdot \Phi^{\mathrm{T}} + \mathbf{Q})\mathbf{H}^{\mathrm{T}} + \mathbf{C}_t^k\\
&\qquad d^k = (\mathbf{z}_t^k - \mu)^{\mathrm{T}} (\mathbf{S}^k)^{-1} (\mathbf{z}_t^k - \mu)\\
&\quad \text{END FOR}\\
&\quad d^j = \min\left(\{d^k\}_{k=1}^{n_k}\right)\\
&\quad \text{IF } d^j \leq \varepsilon\\
&\qquad \mathbf{y} = \mathbf{z}_t^j\\
&\qquad \mathbf{Y} = \mathbf{C}_t^j\\
&\quad \text{ELSE}\\
&\qquad \mathbf{y} = [\,]\\
&\qquad \mathbf{Y} = [\,]\\
&\quad \text{END IF}
\end{aligned}
$$

Algorithm 4: Path association procedure.

$$
\begin{aligned}
&[\mathbf{g}_{t|t}, \mathbf{P}_{t|t}] = \text{KF\_path}\left[\mathbf{g}_{t-1|t-1}, \mathbf{P}_{t-1|t-1}, \mathbf{z}_t^k, \mathbf{C}_t^k\right]\\
&\qquad \textit{Prediction step}:\\
&\qquad \mathbf{g}_{t|t-1} = \Phi \cdot \mathbf{g}_{t-1|t-1}\\
&\qquad \mathbf{P}_{t|t-1} = \Phi \cdot \mathbf{P}_{t-1|t-1} \cdot \Phi^{\mathbf{T}} + \mathbf{Q}\\
&\qquad \text{IF } \mathbf{z}_t^k \neq [\,]\\
&\qquad\quad \mathbf{K}_t = \mathbf{P}_{t|t-1}\mathbf{H}^{\mathbf{T}}\mathbf{S}_t^{-1}\\
&\qquad\quad \mathbf{S}_t = \mathbf{H}\mathbf{P}_{t|t-1}\mathbf{H}^{\mathbf{T}} + \mathbf{C}_t^k\\
&\qquad\quad \textit{Filtering step}:\\
&\qquad\quad \mathbf{g}_{t|t} = \mathbf{g}_{t|t-1} + \mathbf{K}_t\left(\mathbf{z}_t^k - \mathbf{H}\mathbf{g}_{t|t-1}\right)\\
&\qquad\quad \mathbf{P}_{t|t} = \mathbf{P}_{t|t-1} - \mathbf{K}_t \cdot \mathbf{S}_t \cdot \mathbf{K}_t^{\mathrm{T}}\\
&\qquad \text{ELSE}\\
&\qquad\quad \mathbf{g}_{t|t} = \mathbf{g}_{t|t-1}\\
&\qquad\quad \mathbf{P}_{t|t} = \mathbf{P}_{t|t-1}\\
&\qquad \text{END IF}
\end{aligned}
$$

Algorithm 5: Kalman filter for path parameter tracking.

A.3. SIR filter

Algorithm 6 presents the pseudocode of the SIR particle filter. Here, the term $p(\mathbf{s}_t \mid \mathbf{s}_{i,t-1})$ denotes the transitional prior which is chosen instead of optimal importance density. N is the number of samples. The weight $\widetilde{w}_{i,t}$ of each generated sample $\mathbf{s}_{i,t}$ is proportional to the value of the likelihood function given by (26). The weights are normalized before the resampling stage. The detailed information about the resampling procedure as well as the SIR filter can be taken from [13, 23].

A.4. Flow chart of the proposed state space initialization algorithm

In Figure 16 the flow chart of the proposed initialization technique is presented. The multipath association is carried out using the nearest neighbor principle like in Appendix A.1, extended to the multipath case.

$[\hat{\mathbf{s}}_t, \hat{\mathbf{P}}_t^{\mathbf{s}}] = \mathrm{SIR}[\{\mathbf{s}_{i,t-1}\}_{i=1}^{N}, \mathbf{z}_t]$
FOR $i = 1 : N$
$\mathbf{s}_{i,t} \sim p(\mathbf{s}_t \mid \mathbf{s}_{i,t-1})$
$\widetilde{w}_{i,t} = p(\mathbf{z}_t \mid \mathbf{s}_{i,t})$
END FOR
$m = \sum_{i=1}^{N} \widetilde{w}_{i,t}$
FOR $i = 1 : N$
$w_{i,t} = m^{-1} \cdot \widetilde{w}_{i,t}$
END FOR

Algorithm 6: SIR Filter.

Hereby, the squared distances are calculated between all existing path tracks and the actual measured parameters. Beginning with the smallest squared distance corresponding to one measured and tracked path pair, the associations are specified iteratively within the multipath association procedure. Not associated measured paths addressed by the index subset I_0 are used to initialize the new path tracks. The associated measured paths with the indices contained in I are processed by means of the Kalman filter bank. The path track deletion occurs individually for those paths which were not associated during M cycles like in the case with the single path from Section 3.1. Note that only after some delay time T_D which is needed for the detection of the false path tracks and the confirmation of the existing path tracks, the actual MS track initiation occurs via particle filtering technique from Appendix A.3. The result of the sequential state estimation is saved in $\hat{\mathbf{s}}$ and its uncertainty in $\hat{\mathbf{P}}^{\mathbf{s}}$.

ABBREVIATIONS

BS: Base station: it provides the whole spectrum of wireless communication services within cellular network, for example, handling traffic and signaling, transcoding of speech channels, allocation of radio channels to mobile terminals, quality management of transmission, and reception
CIR: Channel impulse response
DoA: Direction of arrival
GPS: Global positioning system
IED: Improvised explosive device
LoS: Line of sight connection
MS: Mobile station: mobile phone or terminal
NLoS: Nonline of sight connection
OS: Observing station: its task is the localization of MSs only. This is the main difference to the BS, which primarily serves for speech and data transfer over the air interface
RSS: Received signal strength
RT: Ray tracing
SIR: Sampling importance resampling
SNR: Signal to noise ratio
SSL: Single station localization
TDoA: Time difference of arrival
ToA: Time of arrival.

REFERENCES

[1] K. W. Kolodziej and J. Hjelm, *Local Positioning Systems: LBS Applications and Services*, Taylor & Francis, New York, NY, USA, 2006.

[2] G. Sun, J. Chen, W. Guo, and K. J. R. Liu, "Signal processing techniques in network-aided positioning: a survey of state-of-the-art positioning designs," *IEEE Signal Processing Magazine*, vol. 22, no. 4, pp. 12–23, 2005.

[3] F. Gustafsson and F. Gunnarsson, "Mobile positioning using wireless networks: possibilities and fundamental limitations based on available wireless network measurements," *IEEE Signal Processing Magazine*, vol. 22, no. 4, pp. 41–53, 2005.

[4] S. Kikuchi, A. Sano, and H. Tsuji, "Blind mobile positioning in urban environment based on ray-tracing analysis," *EURASIP Journal on Applied Signal Processing*, vol. 2006, Article ID 38989, 12 pages, 2006.

[5] A. H. Sayed, A. Tarighat, and N. Khajehnouri, "Network-based wireless location: challenges faced in developing techniques for accurate wireless location information," *IEEE Signal Processing Magazine*, vol. 22, no. 4, pp. 24–40, 2005.

[6] J. J. Caffery, *Wireless Location in CDMA Cellular Radio Systems*, Kluwer Academic, Hingham, Mass, USA, 2000.

[7] T. S. Rappaport, *Wireless Communications: Principles and Practice*, Prentice Hall PTR, Upper Saddle River, NJ, USA, 2002.

[8] L. Cong and W. Zhuang, "Nonline-of-sight error mitigation in mobile location," *IEEE Transactions on Wireless Communications*, vol. 4, no. 2, pp. 560–573, 2005.

[9] M. Layh, U. Reiser, D. Zimmermann, and F. Landstorfer, "Positioning of mobile terminals based on feature extraction from channel impulse responses," in *Proceedings of the 63rd IEEE Semiannual Vehicular Technology Conference (VTC '06)*, vol. 3, pp. 1078–1081, Montreal, Canada, September 2006.

[10] W. D. Wirth, "Direction of arrival estimation with multipath scattering by space-time processing," *Signal Processing*, vol. 84, no. 9, pp. 1677–1688, 2004.

[11] M. Haardt, R. Thomä, and A. Richter, "Multidimensional high-resolution parameter estimation with applications to channel in sounding in high-resolution and robust signal processing," in *High-Resolution and Robust Signal Processing*, Y. Hua, Ed., pp. 253–337, Marcel Dekker, New York, NY, USA, 2003.

[12] Y. Boers and J. N. Driessen, "Multitarget particle filter track before detect application," *IEE Proceedings: Radar, Sonar and Navigation*, vol. 151, no. 6, pp. 351–357, 2004.

[13] B. Ristic, S. Arulampalam, and N. Gordon, *Beyond the Kalman Filter: Particle Filters for Tracking Applications*, Artech House, London, UK, 2004.

[14] D. McNamara, C. Pistorius, and J. Malherbe, *Introduction to the Uniform Geometrical Theory of Diffraction*, Artech House, London, UK, 1990.

[15] J. Maurer, "Strahlenoptisches Kanalmodell für die Fahrzeug-Fahrzeug-Funkkommunikation," Ph.D. dissertation, Universität Karlsruhe, Karlsruhe, Germany, 2005.

[16] W. Koch, "Target tracking," in *Advanced Signal Processing Handbook: Theory and Implementation for Radar, Sonar, and Medical Imaging Real-Time Systems*, S. Stergiopoulos, Ed., CRC Press, Boca Raton, Fla, USA, 2001.

[17] J. Vermaak, S. J. Godsill, and P. Perez, "Monte Carlo filtering for multi-target tracking and data association," *IEEE Transactions on Aerospace and Electronic Systems*, vol. 41, no. 1, pp. 309–332, 2005.

[18] V. Algeier, A. Richter, and R. Thomä, "A gradient based algorithm for path parameter tracking in sounding," in *Proceedings of the 10th Management Committee Meeting (COST273 '04)*, vol. 124, Gothenburg, Sweden, 2004 June.

[19] A. Richter, "On the estimation of radio channel parameters: models and algorithms (RIMAX)," Ph.D. dissertation, Technical University Ilmenau, Ilmenau, Germany, 2005.

[20] R. Thomä, M. Landmann, A. Richter, and U. Trautwein, "Multidimensional high-resolution channel sounding," in *Smart Antennas in Europe—State-of-the-Art*, T. Kaiser, Ed., vol. 3 of *EURASIP Book Series on SP&C*, Hindawi Publishing Corporation, 2005.

[21] Y. Bar-Shalom and T. E. Fortmann, *Tracking and Data Association*, Academic Press, London, UK, 1988.

[22] Y. Bar-Shalom, X. Rong Li, and T. Kirubarajan, *Estimation with Applications to Tracking and Navigation*, John Wiley & Sons, Hoboken, NJ, USA, 2001.

[23] A. Doucet, J. F. G. de Freitas, and N. J. Gordon, *Sequential Monte Carlo Methods in Practice*, Springer, New York, NY, USA, 2001.